The Weaklaw Vent, SE Scotland

The Weaklaw Vent, SE Scotland: Post-eruptive metasomatism of eruptive products by carbo-hydro-fluids of probable mantle origin.

B. G. J. Upton[1], N. Odling[1], L. A. Kirstein[1], J. R. Underhill[2], J. Puziewicz[3], T. Ntaflos[4],

B. Bagiński[5], S. Hillier[6/7], J.C. Andersen[8], G. K. Rollinson[8] and J.-P. Perrillat[9].

[1]School of GeoSciences, University of Edinburgh, West Mains Rd., EH9 3FE, UK.

[2]Centre for Exploration Geoscience, Applied Geosciences Unit, Institute of Petroleum Engineering, School of Energy, Geoscience, Infrastructure & Society, Heriot-Watt University, Edinburgh, EH14 4AS, UK.

[3]Institute of Geological Sciences, University of Wrocław, Pl. M. Borna, 50-204 Wroclaw, Poland.

[4] Department für Lithosphärenforschung, Universität Wien, Althanstrasse 14, 1090 Vienna, Austria.

[5] IGMiP Faculty of Geology, University of Warsaw, al. Żwirky i Wigury 93, 02-089, Warsaw, Poland.

[6] The James Hutton Institute, Aberdeen, AB15 8QH. UK.

[7] Department of Soil and Environment, Swedish University of Agricultural Sciences (SLU), SE-75007, Uppsala, Sweden.

[8] Camborne School of Mines, University of Exeter, Penryn Campus, Tremough, Penryn, TR10 9FE.

[9]Université de Lyon 1, CNRS, UMR 5276, Laboratoire de Lyon, Villeurbanne, F-69622, France.

*E-mail: brian.upton@ed.uc.uk

Abstract. *The Weaklaw vent in SE Scotland (East Lothian coast), inferred to be Namurian, produced lava spatter and volcanic bombs. The latter commonly contained ultramafic xenoliths. All were metasomatized by incompatible element-enriched carbonic fluids. The lavas and xenoliths are inferred to have been basanites and lherzolites prior to metasomatism. The abundance and size of (carbonated) peridotite xenoliths at Weaklaw denotes unusual rapidity of magma ascent and high-energy eruption making Weaklaw exceptional in the British Isles. The lavas and xenoliths were subsequently altered by low-temperature (< 200°) carbo-hydrous fluids to carbonate, clay and quartz assemblages. A small irregular tuffisite 'dyke' that transects the ejecta is also dominantly composed of carbonates and clays. The peridotitic xenoliths are typically foliated, interpreted as originating as mantle shear-planes pre-entrainment.*

Analyses of the relic spinels shows them compositionally similar to spinels in local unaltered lherzolites from near-by basanitic occurrences. Chromium showed neither significant loss nor gain but was concentrated in a di-octahedral smectite allied to volkonskoite. It is in the

complex association of smectite with other clays, chlorite and possibly fuchsite that the assorted incompatible elements are concentrated.

We conclude that late Palaeozoic trans-tensional fault movement caused mantle shearing. Rapid ascent of basanite magma entrained large quantities of sheared lithospheric mantle. Followed by ascent of an aggressive carbonate-/ hydroxyl-rich fluid causing pervasive metasomatism. The vent is unique in several ways: in its remarkable clay mineralogy and in displaying such high Cr-clays in a continental intra-plate setting, in being more productive in terms of its 'cargo' of peridotite xenoliths, in presenting an essentially un-eroded sequence of Namurian extrusives and, not least, for giving evidence for post-eruptive, surface release of small-melt, deep-source fluids.

KEYWORDS: Faulting, basanite, spinel lherzolite xenolith, metasomatism, chrome-rich smectite, tuffisite, rare element transport, mantle de-gassing.

Introduction

The Midland Valley of Scotland is a SW-NE striking Devonian-Carboniferous sedimentary basin bounded to the NW and SE by the Highland Boundary and Southern Uplands Fault systems respectively. Recent research has demonstrated that the basin's syn-tectonic and post-depositional (Variscan) deformation is consistent with a dextral transtensional origin (Underhill *et al*., 2008). That the Weaklaw Vent on the East Lothian coast (*c*.24 km ENE of Edinburgh) lies close to the extrapolated Southern Upland Fault (SUF) (or its closely related Crossgatehall Fault) is considered not to be fortuitous. The vent has remarkable features concerning its volcanology, mineralogy and geochemistry. It was the focus of extensive low-temperature, carbo-hydrothermal metasomatism that, among complex compositional changes to the whole-rock compositions, was the introduction of a wide range of incompatible elements.

The major faults affecting the Firth of Forth in SE Scotland are shown in Fig.1. The SUF, commonly taken to define the southern boundary of the Midland Valley Terrane, separates the lower Palaeozoic (Ordovician) of the Southern Uplands Terrane from the Upper Palaeozoic (Devonian/Carboniferous) terrane of the Midland Valley across most of southern Scotland (Floyd, 1984). However, the SUF is untraceable towards the ENE beyond a point *c*. 20 km south of Edinburgh where it either terminates or has an *en echelon* replacement by the Lammermuir and Dunbar-Gifford Faults (Fig.1). The latter is regarded as a shallow and relatively insignificant feature at depth as may also be the Dunbar-Gifford Fault (Max 1976). It is suggested that the SUF persists north-eastwards beneath the younger Carboniferous of the Midlothian coal-field and that it, or one its splays, controlled the coastal trend between Port Seton and Eyebroughy (Fig.1). To its south-east the Midland Valley Terrane may be overthrust by the Lower Palaeozoic rocks of the Southern Uplands (Bluck 1983; Hall *et al*., 1984), a hypothesis supported by the occurrence of Ordovician high-grade metamorphic xenoliths a few kilometres to the east (Badenszki *et al*., 2009; Badenszki *et al*. 2019).

The north-eastern extrapolation of the SUF, that forms the generally accepted geological southern margin of the Midland Valley, is postulated to pass off-shore between Port Seton and Eyebroughy (Fig.1), (*cf*. Floyd 1994; McKerrow and Elders, 1989; Max, 1976), whilst a fault occupying the same position is referred to as the Firth of Forth fault by Bluck (2002). A further argument favouring the ENE persistence of the SUF (or a related fault) concerns the

extension of a magnetic lineament (characteristic of zones in the Southern Uplands Terrane) that passes close to this coastline. In brief, the crust between the Lammermuir Fault and the hypothesized SUF extension may not be regarded as part of the Midland Valley Terrane but rather as an anomalous sector of the Southern Uplands Terrane (Max, 1976). Strike-slip activity on the boundary fault systems of the Midland Valley resulted in the creation of several NNE-SSW striking folds and several intra-basinal wrench faults including the Ardross, Pentland and Southern Upland Faults. Sub-surface data demonstrate that the fault extension passes to the west of this coast before tipping out to the north-east (Ritchie *et al*., 2003; Underhill *et al*., 2008). We suggest that it passes west of the Weaklaw Vent by less than < 500 m and that late Carboniferous movement along it may have triggered the volcanism.

Fig. 1 about here

The Weaklaw Vent, situated close to the islands of Fidra and Eyebroughy, was a part of the extensive Carboniferous-Permian magmatic activity in Scotland (Kirstein *et al*., 2006). Its most obvious manifestation is as two vertical buttresses, c. 45 m apart and each c. 5 m broad, that stand out from the sea-cliffs (Figs.2 and 3). Locally known as the Hanging Rocks, they are composed of pyroclastic materials. The lava bombs and spatter seen in the Hanging Rocks are most easily examined in the wave-cut platform exposures beneath them. where they are dominantly composed of variably amygdaloidal, globular lava agglutinates and bombs. All have been comprehensively altered to assemblages, dominantly of carbonates and clays. The lavas are commonly rich in spherical/sub-spherical dolomite amygdales, so abundant in some that they appear to have erupted virtually as a froth. The low-temperature alteration of the lavas is such that the original petrography is comprehensively obscured (Figs. 4a and 4b).

Fig.2 about here
Fig.3 about here

Contrasting lithologies, generally darker coloured and typically surrounded by the lava were clearly xenoliths. These are abundant in the Hanging Rocks and the wave-cut platforms beneath them. The xenoliths, (recognised as altered peridotites by Duncan 1972), typically enveloped in ovoid lava coatings, will be referred to as cored bombs. Many of the xenoliths are angular (Fig. 4c) and almost invariably exhibit a planar foliation shown by green schlieren (Fig.4d). Although the silicates are wholly pseudomorphed, a 'ghost petrography' is just discernible though the alteration products. This, together with comparison of relic spinels in the Weaklaw samples (discussed below) with those of fresh peridotites from the Late Carboniferous (possibly Permian?) basanite intrusions in the surrounding area of East Lothian and on Fife (the land lying north of the Firth of Forth, Fig. 1) leaves little room for doubt that Weaklaw, before alteration, had been the site of an eruptive basanite closely comparable petrologically to these others.

The volcanology, indicated by the Weaklaw site was, however, distinct. The Hanging Rocks present unstable cliffs (Fig. 3), the foreshore outcrops are ephemeral subject to the changing cover by sand and seaweed and inland exposures are non-existent. Whilst these problems obviate any detailed study of the anatomy of the Weaklaw volcano the observations allow the following comments. A contact between the Weaklaw deposits and the welded Marine Villa ignimbrites (Visean of the Garleton Hills Volcanic Formation) is indicated

diagrammatically on Fig.2. This contact is interpreted as an unconformity between two very contrasted sequences of pyroclastic rocks. Those to the west are unwelded, well-stratified tuffs with a large percentage of sedimentary clasts together with juvenile mafic clasts. These, probably disturbed by post-consolidation mass-flow, appear to grade westwards into tuffs in which ultramafic clasts increasingly appear on approach towards the Hanging Rocks. We suggest that these belong to a phreatomagmatic cone denoting an early stage of the Weaklaw eruptions before it entered its more productive terminal phase.

The unusual abundance of the mantle xenoliths in and around the Hanging Rocks, coupled with their large sizes (up to 40 cm), testifies to high-energy eruption. The cored bombs and the spatter are evidence of sub-aerial eruption from one of more conduits in the immediate vicinity. We envisage the Hanging Rocks as possibly representing a pair of vertical-sided eruptive conduits that cut the sub-horizontal strata of the early Carboniferous Garleton Hills Volcanic Formation (Figs. 2 and 3). They do not persist seawards and appear to have abrupt northern terminations. If they were conduits cessation of eruption may have been attended by magma withdrawal permitting them to become choked with partially molten material. To have entrained such large (and abundant) mantle samples the magma clearly attained surface level at high velocities, presumably erupting as lava fountains. However, this paper is restricted to describing some of Weaklaw's remarkable mineralogical and geochemical features and must leave any more sophisticated interpretation of the volcano to others.

Figs 4a, 4b, 4c, 4d, 4e about here.

Analytical methods

Major element compositions were determined using an X-ray fluorescence spectrometer at the School of GeoSciences, University of Edinburgh, Scotland. Samples were fused with a lithium metaborate-lithium carbonate flux containing La_2O_3 as a heavy absorber (Johnson Mathey, Spectroflux 105), using a method similar to that developed by Norrish and Hutton (1969). Sample powder was dried at 110°C overnight, and a nominal but precisely weighed 1 g aliquot was ignited at 1100°C to determine loss on ignition (LOI). The residue was then mixed with flux in a sample flux ratio of 1:5 based on the unignited sample weight. The mixture was then fused at 1100°C in Pt 5% Au crucibles in a muffle furnace. After initial fusion, the crucible was re-weighed, and any weight loss from the flux was compensated with additional flux to maintain the 1:5 sample flux ratio as closely as possible. After a second fusion and homogenisation over a Meker burner the molten sample flux mixture was cast onto a graphite mould and flattened with an aluminium plunger. During this process, the mould and plunger were kept at 220°C on a hot-plate.

Trace element concentrations were determined on pressed powder samples. Eight grams of rock powder were mixed thoroughly with eight drops of a 2% solution of polyvinyl alcohol. The mixture was formed into a 40 mm disc backed and surrounded by an aluminium foil cup, by compression between two tungsten carbide discs at a pressure of 1.6 tonnes/cms^2. The fused discs and pressed powder pellets were analysed on a Philips PW2404 X-ray fluorescence spectrometer with a Rh-anode primary X-ray tube. Corrections for matrix effects on the intensities of the major element fluorescence lines were made using theoretical alpha coefficients calculated using Philips software. The coefficients were calculated to allow for the extra flux replacing volatile components in the sample lost during the LOI step, so that

analytical totals should be 100% less the LOI. The spectrometer was calibrated using a suite of ten USGS and CRPG standards the values of which are given in Govindaraju (1994). Calibration lines show that accuracy and precision are closely similar with an average 1σ value across the 10 elements of 0.03 wt.%.

Corrections for the matrix effects on the intensities of major element lines were made using theoretical alpha coefficients calculated on-line using Philips software. The coefficients intensities of the longer wavelength trace element lines (La, Ce, Nd, Cu, Ni, Co, V. Ba and Sc) were corrected for matrix effects using alpha coefficients based on major element concentrations measured at the same time on the powder samples. Matrix corrections were applied to the intensities of the other trace element lines by using the count rate from the $RhK_{\alpha 1}$ Compton scatter line as an internal standard (Reynolds 1963). Line overlap corrections were applied using synthetic standards. The spectrometer was calibrated using USGS and CRPG standards using the values reported by Jochum *et al*. (1990) for Nb and Zr and Govindaraju (1994) for the other elements.

Mineral identification and quantitative phase analysis by X-ray diffraction were done at the School of GeoSciences, University of Edinburgh, using a Bruker-AXS Advance 8 powder diffractometer in a Bragg-Brentano (reflection) geometry, equipped with a Cu tube, (wavelength $K_{\alpha 1}$ = 1.540596 Å), and a NaI detector. Variable slits were used, and the samples were measured in 2 to 65° 2θ range. Identification of minerals was made using Bruker EVA software with reference to the International Centre for Diffraction data PDF-4+ 2015 diffraction database. Quantitative analysis was determined by the Rietveld method (Rietveld 1969) using the computer program Topas 3.1 (from Bruker-AXS).

Complementary work on the clays resulting from hydrothermal alteration was carried out at The James Hutton Institute in Aberdeen. A clay sized fraction of < 2 µm was separated from a vent rock sample for XRD analyses by mounting on a glass slide as an oriented specimen to enhance diffraction from the 001 series. The clay was scanned using Cu radiation. Additionally, the pressed powder pellet (as used for XRF analysis) and a sample of the dyke were McCrone milled and spray-dried to produce random powder specimens, which were quantified by a full pattern fitting method (Omatoso *et al*. 2006).

Electron-microprobe analysis of spinel was by a CAMECA SX5FE at the Department of Lithospheric Research at the University of Vienna. Analyses was conducted under "standard" conditions (acceleration voltage 15 kV, sample current 15 nA, counting times 10 or 20s, natural silicates and synthetic oxides as standards, PAP correction procedure (Pouchou and Pichoir 1991) was applied to all acquired data. Counting times were increased to 40 s to improve detection limits for Ni (*c*. 500 ppm) and Ca (*c*. 300 ppm) in olivine.

QEMSCAN: Major and trace mineral abundances were determined with the QEMSCAN 4300 of the Cambourne School of Mines, Exeter University following the methodology of Gottlieb *et al*. (2000) and Pirrie *et al*. (2004). The analyses included 7.7 million energy dispersive X-ray spectra collected in a 10 µm raster across the thin-section surface. The electron back-scattering coefficient and the interaction of the characteristic X-rays were matched to a spectral database (a modified version of the intellection LCUS SIP) for mineral identification. A comparison of neighbouring spectra forms the basis for identification of particle sizes and mineral associations and the result is visualized in a false-colour image.

The Weaklaw Vent

We apply the term 'Weaklaw Vent' to the narrow (< 200 m) outcrop on the foreshore between low-water and the low sea-cliffs [NT 498 858]. It was mapped by Day (1916; 1923) as

composing a distinctive NE-SW trending strip of volcanic rocks. The Hanging Rocks provide near-vertical sections cutting sub-horizontal pyroclastic and lava units of the Lower Carboniferous Garleton Hills Volcanic Formation (GHVF) (Fig 3), and the foreshore presents a good sub-horizontal section (subject to change according to movement of beach deposits). Some 100 m west of the vent early Visean shales and mudstones crop out: these shallow-water sediments (Fig.2) have been down-faulted against the GHVF although the fault-zone itself is not exposed. According to McAdam and Tulloch (1985) the fault extends NNW-SSE but this conflicts with Day (1916) and air-photographs. We conclude that the vent was probably emplaced along a NE-SW trending fault, as indicated by Day (1916), close to the postulated offshore fault between Port Seton and Eyebroughy. Day (1916; 1923) described the complex strip of vent rocks as comprising an 'intrusion breccia', lying along a NE-SW trending fault, traceable seawards for approximately half-a-kilometre and considered that the 'intrusion' either post-dated the fault or was synchronous with it. Day (1916) also described a thin (< 0.5 m) sill, of vesicular degraded basalt visible only at low-tide, connected to the 'intrusion breccia' within (the Visean) shale and ironstone, hornfelsing the former. Rather than 'degraded basalt' Day (1923) uses the term 'white trap', a quarrymans' and miners' term for hydrothermally altered basalt or dolerite.

According to Francis (1960) the Hanging Rocks are breccias marginal to a neck rather than a basalt intrusion and "that it is difficult, in places, to find a junction between breccia and the neck agglomerate which marginally contains much debris from the surrounding bedded tuffs and agglomerates". Francis (1960) noted the high content of altered basalt in the Hanging Rocks breccia. Although, in part, the vent does consist of a volcanic breccia, most is an agglutinate composed of ovoid to amorphous masses of cream/white, highly altered, lava (Fig. 4a). Many of these masses (up to 1 m across) were volcanic bombs that, together with spatter, accumulated to form what we infer to have been a cone around the paired eruptive vents now composing the Hanging Rocks. The resultant altered basalt is typically rich in near-spherical amygdales (*c*. 1-2 mm diameter) representing vesicles filled by dolomite. Some sub-rounded 'bombs' are so amygdaloidal (Fig.4b) as to represent former basaltic pumices or a magma froth.

XRD analysis shows the 'white trap' to be mainly composed of carbonate (c. 75% modal), dominantly ankerite with subordinate dolomite and calcite, together with < 6% ferro-magnesian phases (antigorite, lizardite and phlogopite). Resistant brown material, commonly present interstitial to the 'white-trap' is largely composed of quartz, ankerite/dolomite with some siderite and subsidiary kaolinite. The vent lacks evidence of having resulted from a phreatomagmatic eruption and is regarded as due to vigorous de-gassing of vapour-saturated magma. Morphologically the ensemble could be taken as surficial eruption products and the present erosional level must be close to the original palaeo-surface.

Mantle xenoliths

A high proportion of the carbonated basaltic bombs contain ultramafic cores ranging up to *c*. 40 cm in diameter (Figs. 4b and 4c) that were initially identified as highly altered mantle xenoliths from the presence of relic Cr-spinel and petrographic indication that they were formerly olivine-rich (Duncan, 1972). The xenoliths have experienced such pervasive carbonation that all high-temperature silicates (presumed to have been olivine, clino- and ortho-pyroxene) have been pseudomorphed, by magnesian carbonates (dolomite and ankerite), clays and quartz. Despite the extensive chemical alteration, petrographic textures remain sufficiently intact under plain polarised light to show an original peridotite fabric. Only

relics of spinel remain of what is inferred to have been the original mineralogy (Duncan, 1972). The only other components in the xenoliths were minute crystals of chalcopyrite and rutile. Whilst the former may have survived from the pre-metasomatised rock, the latter is inferred to be a secondary product of the metasomatism.

Three common characteristics of the 'peridotitic' cores are that they a) commonly have coatings of the altered basalt and appear to have been erupted as 'cored bombs'; b) had cooled enough to have undergone brittle fracture by the time of their entrainment (Fig. 4c); and c) typically possess a marked foliation (Fig.4d), shown by the parallel orientation of pale to dark green schlieren or lenticles (up to 20 mm long and *c.* 2 mm thick) in the creamy-white matrices (Fig.4d). Fig.5 shows a cut-slice of one of the larger metasomatized xenoliths showing the foliation and colour variation. For comparison, a slice of fresh spinel lherzolite is shown to illustrate how the Weaklaw xenoliths may have appeared prior to foliation and recrystallization.

Spinels*:* The yellow-brown spinels in the Weaklaw xenoliths are corroded and embayed and occur only sparsely (Fig. 6a). Their margins are in places spongy with cavities filled by hydrous Al-Si phase(s) (Fig. 6b), however massive margins also occur. The spinels are aluminous (Cr/(Cr+Al) = 0.08-0.09, Table 1) and their composition is uniform across the grains. It is unchanged in the marginal spongy parts which suggests that the minerals were subjected to dissolution and not to chemical alteration that would have affected the composition of the spongy margins (Fig. 6b). This suggests that the spinels probably preserve their primary mantle composition. Spinel has been reported to show comparable resistance to complete dissolution in the altered peridotites of Crommyonia (Greece) (Mitsis *et al*., 2018) and also in the ultramafic enclaves at Almaden (Spain) (Morata *et al*., 2001).

The composition of the spinel (Table 1) resembles that of the spinels in fresh peridotite xenoliths from the near-by Brigs of Fidra basanite (Downes *et al*., 2001) and those of the basanitic neck at Ruddon's Point, close to the Ardross Fault, Fig.1. (Upton *et al*., 2011). The similarity is sufficient for us to claim that the Weaklaw xenoliths were, prior to metasomatism, comparable to the spinel lherzolites common in basanite intrusions and diatremes elsewhere in East Lothian and in Fife (Fig.1: Upton *et al*., 2011).

Figs. 6a and 6b about here

(Table 1 about here)

Clays*:* Whereas the clay patches within the altered peridotite are typically colourless in plain-polarised light some show, to varying degrees of intensity, a blue-green colouration. Such clays are commonly found adjacent to the corroded spinel margins and are found by scanning electron microscope to have Cr_2O_3 values up to 10 wt%. The clays and carbonates tend to be complexly intergrown (Fig.6a). This assemblage is inferred to have resulted from reaction between CO_2 and forsteritic olivine and also from reaction with the pyroxenes and partial reaction with the spinel. XRD analyses of the green schlieren show them to be a complex fine-grained association of clays, chlorites, carbonates and (opaline) quartz. In a high-magnification image the crystalline form of some of the clays can be seen, with kaolinite and smectite crystals distinguishable (Fig.7).

Fig.7 about here

An attempt to hand-pick the darker green components from crushed schlieren material under water (for improved colour discrimination) for XRF analysis failed as they promptly disaggregated into a green (assumed) colloidal solution. The inference is that the clay component undergoes rapid hydration causing loss of coherence and dissemination into nano-particles. After evaporation of the 'solution' the evaporite was analysed by XRF (Table 2). It has c. 27 wt% loss on ignition with a high concentration of Cr (11,360 ppm). Whilst the K_2O content is 0.19 wt%, the concentrations of Rb (44 ppm) and Ba (1105 ppm) are also notably higher than in the whole-rocks by factors of approximately 5 and 22 times respectively. Very chrome-rich smectite, volkonskoite, from the Akerman area in Russia, has been described as being associated with colloidal, organic carbon-bearing chromium allophanoids (Gudoshnikov et al., 1968; Foord et al., 1987), we suggest that a comparable association exists in the Weaklaw chrome-clays.

No satisfactory analysis by electron micro-probe could be made on account of the material being very fine-grained and poly-mineralic. However, one species of phyllosilicate, analysed by microprobe gave K_2O values ranging from 2.99 to 4.76 wt%. Such a large ion lithophile element (LILE) may be accommodated in Cr-muscovite (fuchsite) although this was not detected by X-ray diffraction. In the three chemical analyses (evaporite, 'random powder' as used for XRF and in the < 2µm clay fraction) the values for LILE, although differing widely, range up to 0.78 K_2O%, 1488 ppm Rb, 7 ppm Cs, and 1488 ppm Ba, collectively indicate the significant presence of LILE. Again, relying on the translation from Aleksandrov *et al*. (1940) in Foord *et al*. (1987), high-Cr clay, volkonskoite was identified as a heterogeneous mixture including crypto-crystalline silica, kaolinite and adsorbed alkaline earth elements. We suggest that the alkali and alkaline earth elements reported in Table 2 may likewise be adsorbed onto the Cr-rich clays. Mitsis *et al*. (2018) also noted an enrichment in LILE (specifically Rb and Ba) in Cr-bearing clays from altered ophiolitic rocks in Greece. In the Weaklaw schlieren chromium reaches its highest concentration in the <2µm clay fraction (Table 2). We conclude that chromium from former Cr-spinel and Cr-diopside was scavenged by the metasomatic agent and re-precipitated as smectitic clays: some of the latter may classify as volkonskoite (Foord *et al*. 1987) though more generally they are Cr-montmorillonite or Cr-beidellite. Analyses of the Weaklaw Cr-clay concentrates (Table 2) also show Ni, Co and V contents up to 348, 158 and 2432 ppm respectively. Other 'exotic' trace components that would not have been expected in a peridotite include Pb (533 ppm) and P (1082 ppm: Table 2). We conclude that the green clays in the ultrabasic xenoliths at Weaklaw, whilst being dominantly Cr-smectites, are complex and merit further investigation.

(Table 2 about here)

Whole-rock compositional changes due to metasomatism

At Brigs of Fidra (Fig.2) the peridotite xenoliths are hosted by intrusive basanite (Downes *et al*., 2001). Since mantle xenoliths on both sides of the Firth of Forth are contained in basanitic intrusions or vents, the assumption that the Weaklaw xenoliths were brought up by basanite magma similar to that of Fidra and Brigs of Fidra a few hundred metres to the east. (From here on the terms 'metasomatised peridotite' and 'metasomatised basalt' will be contracted to 'meta-peridotite' and 'meta-basalt' despite the inferred low-temperature nature of the recrystallisation). Comparison of the meta-peridotite composition with that of the un-altered Brigs of Fidra peridotite (Table 3;) shows that among the major elements the Weaklaw samples have undergone extensive loss of Si, Ti, Mg and Na but addition or enhancement of

Al, Fe, Mn and Ca. For the meta-basalt, in comparison with the fresh basanite from the Brigs of Fidra intrusion (Fig.2), alteration led to depletion of Si, Ti, Al, Fe, Na and (slightly) K and gain in Ca and Mn. The high carbonate content of the metasomatised rocks indicates that CO_2 was a dominant component of the metasomatizing agent.

(Table 3 about here)

*Th*e enrichment of the meta-peridotite in Fe, Mn, Ca, Sr and volatiles would be expected as a natural outcome of the loss of Si, Mg etc. whereas Increase in Cr, V and Sc may reflect re-distribution of elements from the host basanite. Mitsis *et al*. (2018) note that Cr-bearing clays produced by metasomatic alteration of ultramafic rocks can be highly enriched in a range of elements including V and Sc. However, the increases in Rb, Ba, Zr, Nb, Pb and LREE, relative to their concentrations in the (supposed fresh analogue) peridotite, are attributed to their introduction by the metasomatising agent.

Consideration of the compositions of the meta-basanite compared to the fresh basanite indicates that the alteration subtracted Ba, Sr and Nb but added Ni, Cu, Pb, U and Th. There appears to have been a fall in the Th/U ratio from *c*.3.7 (fresh basanite) to c. 0.3 (metasomatised basanite; Fig.8). The ratios of Zr/Nb and Y/Ce tend to be relatively robust with respect to alteration processes: the metasomatism caused little change in Zr/Nb ratios in the host: 4.31 in the fresh basanite and 4.39 in the meta-basalt. Alteration of the basanite caused reduction of the Y/Ce ratio from 0.33 to 0.28, implying either Y loss or Ce gain. There was also Y/Ce reduction in the peridotite xenoliths from 3.08 to (a mean of) 0.34 brought about by metasomatism.

Fig.8 about here

Carbonate-rich tuffisite. A dyke-like feature, up to 30 cm wide, cross-cuts the Weaklaw vent (Fig. 9a) The width and orientation changes across the outcrop. Lacking fine-grained chilled-margins it appears not to be a magmatic dyke but more akin to the tuff dykes (tuffisites) described from this part of the coast by Francis (1960). However, it differs from the latter in lacking wall-rock materials and its most distinctive characteristic is its content of white fragments, up to 60-70% modally that do not exceed 5 mm across and are homogeneous, anhedral and typically angular (Figs.9a and 9b): superficially they resemble feldspar phenocrysts. They are opaque in thin-section and XRD analysis shows them to consist predominantly of kaolinite and illite (with the former exceeding the latter by a factor of 10). We suggest that they originated as alkali feldspars that were subsequently pseudomorphed and broken during rapid emplacement by a fluid.

(Figs.9a and 9b about here)

Petrographically there are some indications of a flow-pattern in the tuffisite. Additional to the supposed feldspar pseudomorphs the dyke contains small sub-rounded clasts (up to 10 mm) with colours varying from black to brown and white. The speckled dyke interior grades into more homogenous brown material, the colouring of which is ascribed to its content of goethite. Whole-rock XRF analyses of samples from the tuffisite and its marginal brown facies are presented in Table 3. SiO_2 ranges from 48 - 58 wt%, with approximately 20 - 24 wt% Al_2O_3, 2 – 5 wt% Fe_2O_3, 3 - 6.5 wt% CaO and 11 - 16 wt% LOI. Although there is variability among the trace-elements, concentrations of Zr, Nb, Y, LREE, U and Th are consistently high (Table 3). Zr and Nb exhibit values of 2560 ppm and 305 ppm respectively (with a Zr/Nb of 8.83).

The LREE (La, Ce and Nd) summations range from 630 – 817 ppm; Th 46 - 56 ppm and U from 3 - 5 ppm (mean Th/U is 13). In brief, the speckled tuffisite samples show higher values of Zr, Nb, Y, LREE and Th than any other samples in this study. The dyke matrix is very fine-grained. Use of QUEMSCAN indicates a zircon modal content in one thin-section of 0.24% (median grain-size c. 45µm). Ilmenite, rutile and niobo-rutile (ilmenorutile) are predominantly associated with the carbonate. Niobo-rutile (0.2% modal) is the presumed principal host for Nb whilst apatite and zircon are likely to host the REE.

The goethite-rich marginal facies lacking the white-speckles has notably high Ni (350 ppm) and Zn (290 ppm). Relative to the speckled central facies, Ba and the HFSE contents are much reduced in the marginal sample whilst Sr is distinctly higher. This trace element behaviour is consistent with fluid interaction, mobilisation and residual enrichment. LILE are known to be mobilised by high and low temperature alteration processes (Kirstein *et al*., 2006). In particular, high and low temperature fluids rich in CO_2 and H_2O can promote LILE and HFSE element mobilisation (Berkesi *et al*., 2012; Humphris and Thompson, 1978).

The 'dyke' also contains sparse anhedral but crudely isometric clasts up to 10 mm diameter that appear homogeneous but with colours varying from dark brown, through pale brown to creamy-white (Fig.9b). Powders drilled from three examples across this colour spectrum were also analysed by XRD. According to the XRD results the darkest clast is composed mostly of carbonate (calcite and dolomite), with c. 9% feldspar and <2% clays. The pale brown clast has less than half as much carbonate together with c. 37% feldspar and c. 23% clay whilst the creamy-white clast has <3% carbonate but 63% feldspar and c. 29% clay. All three could have been dominantly composed of feldspar but exhibiting varying degrees of carbonation and hydration. The average material from the speckled dyke central facies is composed of *c*. 56% carbonate (roughly equal amounts of calcite, dolomite and ankerite) and *c*. 33% clays (dominantly kaolinite). The remaining 10% is composed of quartz, anorthite, microcline, orthoclase, ilmenite, goethite and zircon with none exceeding 3%. Material drilled from the matrix surrounding the white fragments comprises *c*. 89% carbonate (dominantly calcite).

Discussion

Xenolithic evidence on the deep structure of East Lothian*:* The distribution of localities where magmas have brought up xenoliths of mantle and/or deep crustal lithologies supports the contention that there is a major crustal dislocation west of East Lothian. At Partan Craig, c. 7 km east of Weaklaw, xenoliths of high-grade gneisses (Graham and Upton, 1978), recently identified as having late Ordovician (and possibly lower Silurian) ages (Badenszki *et al*., 2019), underlie the upper Palaeozoic successions. Within the Weaklaw Vent itself small (< 15 mm) fragments of high-grade metamorphic rocks (graphitic quartzo-feldspathic gneisses) have been found (pers. comm. Peder Aspen). On the supposition that these too are Ordovician, they support the contention that the fault block between the extrapolated SUF trace and the Dunbar-Gifford and Lammermuir Faults composes part of the Southern Uplands rather than the Midland Valley terrane (Max, 1976). Offset a few kilometres to the north and west of the extrapolated SUF is the trace of the Ardross Fault (Fig.1). Spinel lherzolite xenoliths occur in late Carboniferous vents along the latter but are unknown between these faults. The xenolith distribution may be taken to provide supplementary evidence that the change of orientation of the Port Seton-Weaklaw coastline relates to the terrane boundary (Max, 1976).

***Chronological implications**:* Mantle xenolith localities in Scotland are widely distributed around the north, west and south of Scotland (Upton *et al*., 1983). The features of the Weaklaw xenoliths, however, render them unique. The vent is dominantly filled by basaltic bombs that were subsequently recrystallised and the presence of mantle xenoliths in a presumed former silica-deficient basaltic host indicates closer affiliation to the later Carboniferous alkali dolerite (basanitic) sills of East Lothian than to the 'transitional' olivine basalts typical of the Visean. Although precise dating has yet to be made on any of the East Lothian alkali dolerite intrusions, their stratigraphic relationships suggest their ages to be tens of millions of years younger than the Dinantian volcanism. The East Lothian mafic intrusions are comparable to the late intrusions in Fife for which a Namurian or younger age has been proposed (Forsyth and Chisholm, 1977). However, a K-Ar age quoted in Downes *et al*. (2001) for Fidra is 264 ± 10 Ma which, if substantiated, would make it Permian. The precise age is irrelevant here other than to suggest that the Weaklaw eruption is many millions of years younger than the Visean Garleton Hills Volcanic Formation that it intercepts. The tuffisite and metasomatism are likely to have been pene-contemporaneous.

Whereas the alkali dolerites sills (*e.g.* Fidra) along this coast were trapped in Carboniferous strata, the Weaklaw magma clearly reached the surface. The vent products in and around the Hanging Rocks contain a prolific amount of the ultramafic inclusions that make Weaklaw outstanding among the many other Scottish xenolith locations. Both the quantity and size of the entrained peridotite samples imply a greater ascent rate for the host magma than at any other site in the British Isles. Its lack of recognition until that by Duncan (1972) is undoubtedly due to the subsequent carbonation that precluded discovery. The composition of the protolith is considered to have approximated that of the spinel lherzolites at Brigs of Fidra regarded as typical for the lithospheric mantle in the region (Downes *et al*., 2001). The agglutinated assemblage of highly vesicular bombs resembles that of surficial eruptive products implying that the exposure probably reflects an erosional depth of less than a few tens of metres. Accordingly, consideration of the outcrop on the foreshore as (very roughly) approximating to a palaeo-surface the metasomatic fluid must, at this level, have been gaseous. If so the post-eruptive hydrothermal flux would likely have been manifest in fumarolic activity (*cf*. Mitsis *et al*., 2018). We contend that the Weaklaw phenomena may have been triggered by late Carboniferous (or Early Permian (?) trans-tensional movement of the postulated fault which a) promoted adiabatic mantle melting, b) provided a channel for magma ascent and c) sheared the peridotite.

The relatively high contents of HFSE, LREE and actinide elements in the cross-cutting tuffisite dyke and, to a lesser degree in the peridotites, invites speculation concerning the source of the metasomatic fluid. The crust beneath Weaklaw is approximately 30 km thick of which the uppermost c. 3 km is of arenaceous lower Carboniferous and 'Old Red Sandstone' (i.e. Devonian and Upper Silurian). Xenolithic evidence indicates that these overlie lower Palaeozoic, largely calc-alkaline igneous rocks (Badenszki *et al*., 2019). The composition of the lower crust (c. 15km thick (Bamford *et al*., 1977), inferred from xenolithic evidence (Downes *et al*. 2001; Upton *et a*l. 2011) is dominantly made of meta-dioritic and meta-gabbroic cumulates. Since none of these sub-Weaklaw crustal rocks is a likely source for the incompatible element-rich carbonic fluid, the most plausible hypothesis is that it arose from small-melt fractions in the mantle.

***Structural implications**:* The NE-SW trend of the coast west of Weaklaw is roughly co-linear with the offshore trace of the Southern Upland fault (or its closely-related Crossgatehall Fault:

Fig.1). Lying between this and the paired Dunbar-Gifford and Lammermuir Faults is the East Lothian fault-block in which deep-source xenoliths are comparatively common whereas they are unknown further to the north-west until the Ardross Fault is reached. The basanitic magmas responsible for the dolerite sills and minor intrusions along the coast between Port Seton and Weaklaw (Williamson 2003; Howells 1969) are probably also related to the postulated off-shore NE-SW fault zone. Additionally there are five cryptovents occurring along this coast containing intrusive tuffs and breccias containing vesicular, devitrified glassy particles. Some of the cryptovents give evidence for initial uplift and post-eruptive collapse suggesting high-pressure discharge of gas or super-critical fluid. That the matrices to the tuffisites and breccias comprise carbonate and kaolinite provides some reason to consider them affiliated with the Weaklaw phenomena.

Geochemistry and mineralogy of the xenoliths: The foliation characteristic of the Weaklaw xenoliths is ubiquitous (Figs. 4d and 5). It pre-dated their entrainment and may reflect shearing of the protolith caused by movement on the hypothetical off-shore fault (Fig.1). The green colouration of the schlieren is due to one or more Cr-rich clays (smectites) resulting from dissolution and reprecipitation of chromium from the former peridotite. Both Ce and U are redox-sensitive and can be preferentially enriched during fluid-rock reactions due to oxidation to Ce(IV) and U(VI). The introduction of Rb, Ba, Sr, Zr, Nb, Y, Pb and LREE to the peridotites was due to the metasomatism. The trace element behaviour is consistent with an interaction of the rocks with CO_2 and probably halogen–rich fluids, resulting in differential additions and leachings, possibly due to complex ion formation (Bau, 1996).

Comparable situations where Cr-rich phyllosilicates have been recrystallised by metasomatic fluids in hydrothermally-altered ultramafic associations have been described, e.g. by Mitsis *et al*. (2018). The ophiolitic rocks experienced hydrothermal alteration that leached different elements in relation to 'intense post volcanic activity' (Mitsis *et al.* 2018), a phenomenon that probably occurred at Weaklaw. The Cr_2O_3 content of some of the resultant clays reaches c. 14 wt% and they were also enriched in As, Se, Ni, V, Sc and Tl but depleted in LILE, HFSE and in Cu and Zn. The alteration of minerals in serpentinites through post-volcanic hydrothermal activity was accomplished via geothermal degassing in a strongly acid environment that led to the mobility of some elements (Mitsis *et al.,* 2018)**.** Spinel was highly susceptible to the alteration losing Al, Cr, Fe and Mg as were the olivines that lost Fe, Mg and Si. In another comparable situation in Spain, Morata *et al*. (2001) record the generation of fuchsite and Cr-rich chlorites and illites in hydrothermally-altered ultramafic enclaves in which former Cr-spinels had reacted under highly acid conditions (pH < 0.3), losing Al, Cr, Fe, and Mg. The liberated Cr^{3+} was accommodated in octahedral suites in the clay lattices. At Weaklaw post-eruptive alteration by carbo-hydrothermal processes enriched the lherzolites in incompatible elements from Rb to Nd, whereas the host basanite was most notably enriched in U.

The cross-cutting carbonate/clay-rich Weaklaw tuffisite has a remarkable concentration of Zr, Nb, Y, LREE, U and Th. We presume that the tuffisite shared the same metasomatic event as the basanite and its xenoliths but we have no knowledge of its pre-metasomatic geochemistry and mineralogy. The alteration of the Weaklaw rocks was so comprehensive that passage of the metasomatizing fluids is likely to have continued over a substantial period. Judging from data on mineral alteration in hydrothermal systems (Reyes, 2000) it is probable that the Weaklaw fluids were acidic with temperatures between 100-200°C. As noted above

both Mitsis *et al.* (2018) and Morata *et al*. (2001) considered that the metasomatic fluids in their respective Greek and Spanish occurrences had been acidic.

The wide variation in the resultant geochemistry of the Weaklaw meta-peridotites and meta-basanites was presumably dictated by the initial permeability and porosity of their un-metamorphosed precursors, characteristics linked to their physical and chemical differences. The peridotite would have been a coarse-grained holocrystalline rock whereas the basanite was largely glassy or micro-crystalline. The gross disparity in their initial major element compositions (Al, Mg, Ca and Na) and trace-element (Ni, Cr, V, Sc, Ba, Sr and HFSE) would also have been a factor determining which elements were preferentially redistributed. The data suggest that the fluids donated K, Rb, Ba, Sr, Pb, Zr, Nb, LREE etc., indicating that the metasomatism could not have been due to reactivated ground-waters alone. Whilst ground-waters were most likely involved as dilutants, a deep-source CO_2-rich component was presumably implicated. The introduction of rare-earth and other 'exotic' elements further hints at their complexing with fluorine (Kirstein *et al.* 2001) although we have no independent evidence for this. However, a recent account of post-magmatic expulsion of fluids rich in F and CO_2 metasomatising local rocks suggests a parallel with the Weaklaw phenomena (Ranta *et al*. 2018). These authors describe a 55 m-wide dolerite dyke in the Grønnedal-Ika alkaline complex, South Greenland, intruded into carbonatite, that acted as a conduit for hydrothermal fluids. The fluids altered the composition of the surrounding carbonatite up to a distance of 40 m. Light rare-earth elements, Nb, Ta, Sr, Mn and P were mobilised and (primary) siderite was oxidised to magnetite.

The high concentrations of Zr, Nb, Y, REE, U and Th in the Weaklaw tuffisite are particularly enigmatic. If our interpretation that the white clay-rich clasts in the dyke are chemically and mechanically degraded alkali feldspars is correct then the associated high field-strength element concentration is consistent with the (hypothetical) feldspars having been derived from volatile-rich per-aluminous magmas (Upton *et al*., 2009) with a significant volatile component. The enrichment in HFSE has been speculatively attributed to scavenging and subsequent concentration of incompatible elements by fluxing of CO_2-rich fluids in the lithospheric mantle. The only other concentration of Zr, REE, Nb and Th known in south-central Scotland is that of a xenolith (amongst a suite of spinel lherzolites and pyroxenites) from Ruddon's Point in the vicinity of the Ardross Fault, Fife (Aspen *et al*. 1990: Upton *et al*. 2009) composed of anorthoclase, corundum, zircon, apatite and yttro-niobate. Its crystallisation was attributed to enriched fluids ascending through the lithospheric mantle in advance of the basanite host magma. At Weaklaw, however, this inferred sequence is reversed. The relationship of the Weaklaw and Ruddon's Point enrichments is not known but we suggest they may be closely related.

Summary

The major faults, including the Southern Upland Fault, splay out within the recently-formed Laurussian continent, forming a rift valley across the Lothians, widening NE from *c*. 10 to *c*. 18 km and bounding the Southern Uplands terrane (Fig.1). During the later Carboniferous, lithospheric trans-tension promoted small-scale mantle melting, producing basanitic magmas. Some of these, ascending via the inferred off-shore fault zone, intruded Carboniferous strata as sills but at Weaklaw they erupted sub-aerially. The peridotitic cores to many of the basaltic bombs in the Weaklaw vent are regarded as retrograded analogues of the fresh rocks occurring nearby on Fidra Island. The ubiquitous foliation (schlieren) in the

xenoliths is regarded as originating through mantle shearing, as evidenced in some of the xenoliths brought up by vents along the (Fife) Ardross Fault (Chapman 1976). The characteristic green colour of these schlieren is due a complex of chrome-rich clays, predominantly di-octahedal smectite. Vent eruption was followed by intrusion of a small tuffisite body, principally composed of clays and carbonates, containing 'sharp' kaolinite-rich clasts inferred to have resulted from mechanical break-down of alkali feldspars. Whole-rock analyses of the tuffisite showed enhanced contents of Zr, Nb, Y, REE, U and Th. Whilst its petrogenesis remains enigmatic, we suggest that these trace elements were introduced by a CO_2 and probably halogen-rich metasomatic fluid.

The Weaklaw vent is considered have been the site of an unusually high-energy eruption, followed by prolonged passage of chemically aggressive carbonic fluids. The siting and orientation of the Weaklaw Vent, in conjunction with its content of sheared mantle xenoliths prompts the speculation that it was associated with the SUF. Right-lateral trans-tensional movement of the latter affected strata up to, and including, the Visean but diminished in the Namurian and Westphalian. West of Weaklaw the coast-line swings from an approximately WNW-ESE orientation to NE-SW, making it essentially co-linear with the trace of the hypothetical fault, suggesting that the geography has been fault-controlled. A linear magnetic anomaly (indicated diagrammatically in Fig. 1) is coincident with this lineament (Max 1976). The occurrence of Ordovician meta-igneous xenoliths in a vent c. 7 km east of Weaklaw (Badenszki *et al*., 2019; Upton *et al*., 1976) suggests that the fault marks the northerly limit of Ordovician rocks at relatively shallow depth, defining the terrane boundary between the Southern Uplands and the Scottish Midland Valley.

Because the Weaklaw metasomatic fluid was reacting with sub-aerial eruptive products we suggest that the term mantle 'de-gassing' is not inappropriate for the phenomena described above. The un-preposessing appearance of the rocks, camouflaged by the secondary alteration, was doubtless a principal reason for their neglect. None-the-less Weaklaw has a number of unique features that invite further study.

Acknowledgements
Assistance in the field from W. Gilmour and C. Pin is gratefully acknowledged. We are grateful to G.O. Fridleifsson for advice concerning the low-temperature alteration and to E. Badenszki and F. Albarede for helpful comments. We thank Stavros Vrachiotis (for collecting the drone footage that added to our understanding of the Hanging Rocks) and also to Sandra Mather for map drafting and Zoe Hamill for photography. We are grateful to our three reviewers whose criticisms helped revision of the manuscript.

References

ALEKSANDROV, V.V., IGNAT'EV, N.A. and KOBJAK, G.G. (1940) Volkonskoite of the Kama region. *Ucheniye Zapiski Molatovskogho Gousdarstvennogo Universita imeni, A.M. Gor'ogo* 4, pt. 34, 5 – 77 (in Russian).

ARAI, S. (1994) Characterisation of spinel lherzolites by olivine-spinel compositional relationships. Review and interpretation. *Chemical Geology*, **113**, 191-204.

BADENSZKI, E., DALY, J.S., HORSTWOOD, M.S.A., WHITEHOUSE, M.J., KRONZ, A. and UPTON, B.G.J. Deep crustal meta-igneous xenoliths from the Scottish Midland Valley: vestiges of a Late Ordovician (to Mid-Silurian?) arc and Early Devonian Granite Magmatism. *Journal of Petrology*. *(Submitted).*

BAMFORD, D., NUNK, K., PRODEHL, C. and JACOB, B. 1977. LISPB-lll Upper crustal structure of Northern Britain. *Journal of he Geological Society, London.* **131**, 481-498.

BAU, M. (1996) Controls on the fractionation of isovalent trace elements in magmatic and aqueous systems: evidence from Y/Ho, Zr/Hf and lanthanide tetrad effect. *Contributions to Mineralogy and Petrology*, **123** (3), 323-333.

BERKESI, M., GUZMICS, T., SZABÓ, C., DUBESSY, J., BODNAR, R.J., HIDAS, K. and RATTER K. (2012) The role of CO_2-rich fluids in trace element transport and metasomatism in the lithospheric mantle beneath the Central Pannonian Basin, Hungary, based on fluid inclusions in mantle xenoliths. *Earth and Planetary Science Letters*, **331–332**, 8-20.

BLUCK, B.J. (1983) Role of the Midland Valley of Scotland in the Caledonian Orogeny. *Transactions of the Royal Society of Edinburgh: Earth Sciences*, **74**, 119 –136.

BLUCK, B.J. (2002) The Midland Valley Terrane. In: N.H. TREWIN ed. *The Geology of Scotland*, 4th edition, The Geological Society, London. 149-166.

CHAPMAN, N.A. (1976) Inclusions and megacrysts from undersaturated tuffs and basanites, East Fife, Scotland. *Journal of Petrology* **17**, 472-498.

CLOUGH, C.T., BARROW, G., CRAMPTON, C.B., MAUFE, H.B., **B**AILEY, E.B. and ANDERSON, E.M. (1910) The geology of East Lothian 2nd edition, *Memoir of the Geological Survey of Scotland.*

DAY, T.D., (1916) The breccias of Cheese Bay and the "Yellow Conglomerates" of Weak Law. *Transactions of the Edinburgh Geological Society* **10**, 261-275.

DAY, T.C. (1923) A new volcanic vent and other new geological features on the shore, Weak Law, near Gullane. *Transactions of the Geological Society of Edinburgh* **11**, 185-199.

DOWNES, H., UPTON, B.G.J., HANDISYDE, E and THIRLWALL, M.F. (2001) Geochemistry of mafic and ultramafic xenoliths from Fidra (Southern Uplands, Scotland): implications for lithospheric processes in Permo-Carboniferous times. *Lithos,* **58**, 103-124.

DUNCAN, A.M. (1972) The occurrence of an ultramafic xenolith in the vent at Weak Law Rocks, East Lothian. *Journal of the Arthur Holmes Society (Durham)* **5-1**, 31-36.

FLOYD, J.D. (1994) The derivation and definition of the 'Southern Upland Fault: a review of the Midland Valley-Southern Uplands terrane boundary. *Scottish Journal of Geology*, **30**, 51-92.

FOORD, E.E., STARKEY, H.C., TAGGART, jnr, H.C. and SHAWE, D.R. (1987) Reassessment of the volkonskoite—chromian smectite nomenclature problem. *Clays and Clay Minerals*, **35**. No.2, 139-149.

FORSYTH, I.H. and CHISHOLM, J.I. (1977) The Geology of East Fife, *Memoir of the Geological Survey, Great Britain.*

FRANCIS, E.H. (1960) Intrusive tuffs related to the Firth of Forth volcanoes. *Transactions of the Edinburgh Geological Society*, **18**, 32-50.

FRANCIS, E.H. and HOPGOOD, A.M. (1970) Volcanism and the Ardross Fault, Fife. *Scottish Journal of Geology* **6**, 162-185.

GOTTLIEB, P., WILKIE, G., SUTHERLAND, D., HO-TUN, E., SUTHERS, S., PERERA, K., JENKINS, B., SPENCER, S., BUTCHER, A., RAYNER, J. (2000) Using quantitative electron microscopy for process mineralogy applications. *Journal of the Minerals, Metals and Materials Society* **52**(4), 24-25.

GOVINDARAJU, K. (1994) Compilation of working values and sample description for 383 geostandards. *Geostandards Newsletter* **18**: Special Issue.

GRAHAM, A. and UPTON, B.G.J. (1978) Petrology of gneisses in diatremes, Scottish Midland Valley. *Journal of the Geological Society of London*, **135**, 219-228.

GUDOSHNIKOV, V.V., IGNAT'EV, N.A. and KISELEV, G.N. (1968) Volkonskoite and chromian allophanoids in Jurassic formations of the Akerman area. *Ucheniye zapiski Permskogo Ordena Trud. Krasnogo Znameni Godsudarst-vennogo Univ. imeni A.M. Gor'kogo, Geol. Petrograf. Zapadnogo Urala* **4**, No. 182, 47-62 (in Russian)

HALL, J., BREWER, J.A., MATHEWS, D.H. and WARNER, D.R. (1984) Crustal structure across the Caledonides from the WINCH seismic reflection profile: influences on the evolution of the Midland Valley of Scotland. *Transactions of the Royal Society of Edinburgh: Earth Sciences*, **75**, 97-109.

HOWELLS, M.F. (1969) Cryptovents and allied structures in Carboniferous strata between Port Seton and Aberlady, East Lothian. *Scottish Journal of Geology*, **5**, 1-10.

HUMPHRIS, S.E. and THOMPSON, G. (1978) Trace element mobility during hydrothermal alteration of oceanic basalts. *Geochimica et Cosmochimica Acta*, **42**(1), 127-136.

JOCHUM, K.P., SEUFERT, H.M. and THIRLWALL, M.F. (1990) High-sensitivity Nb analysis by spark-source mass spectrometry (SSMS) and calibration of XRF Nb and Zr. *Chemical Geology*, **81** (1-2), 1-16.

KIRSTEIN, L.A., DAVIES, G.R. and HEEREMANS, M. (2006) The petrogenesis of Carboniferous–Permian dyke and sill intrusions across northern Europe. *Contributions to Mineralogy and Petrology*, **152**, 721-742.

KIRSTEIN, LA, HAWKESWORTH, C & GARLAND, F. (2001) Silicic lavas versus Rheomorphic ignimbrites: A chemical distinction? *Contributions to Mineralogy and Petrology*, **142**, 309-322.

MAX, M.D. (1976) The pre-Palaeozoic basement in south-eastern Scotland and the southern upland fault. *Nature*, **264**, 485-486.

McADAM, A.D. and TULLOCH, W. (1985) Geology of the Haddington District. Memoir of the British Geological Survey, Sheet 33W and part of 41 (Scotland).

McKERROW, W.S. and ELDERS, C.F. (1989) Movements of the Southern Upland fault. *Geological Journal of the Geological Society, London*. 146, 393-395.

McINTYRE, R.M., CLIFF, R.A. and CHAPMAN, N.A. (1981) Geochronological evidence for phased volcanic activity in Fife and Caithness necks. *Transactions of the Royal Society of Edinburgh, Earth Sciences*, **72**, 1-7.

MITSIS, I., GODELITSAS, A., GÖTTLICHER, J., STEININGER, R., GAMELETSOS, P.N., PERRAKI, M., ABAD-ORTEGA, M.M. and STAMATAKIS, M. (2018) Chromium-bearing clays in altered ophiolitic rocks from Crommyonia (Soussaki) volcanic area, Attica, Greece. *Applied Clay Science*, 362-374.

MORATA, D., HIGUERAS, P., DOMINGUEZ_BELLA, S., PARRAS, J., VELASCO, F. and APARICIO, P. (2001) Fuchsite and other Cr-rich phyllosilicates in ultramafic enclaves from the Alamaden mercury mining district Spain. *Clay Minerals*, **36**, 345-354.

NORRISH, K. and HUTTON, J.T. (1969) An accurate X-ray spectrographic method for analysis of a wide range of geological materials. *Geochimica Cosmochimica Acta,* **33,** 431-453.

OMATOSO, O., McCARTY, D., K., HILLIER, S. and KLEEBERG, R. (2006) Some successful approaches to quantitative mineral analysis as revealed by the 3rd Reynolds Cup contest. *Clays and Clay Minerals*, **54**, 748-760.

PIRRIE, D., BUTCHER, A.R., POWER, M.R., GOTTLIEB, P., MILLER, G.L. (2004) Rapid quantitative mineral and phase analysis using automated scanning electron microscopy (QEMSCAN®); potential applications in forensic geoscience. In: Pye, K., Croft, D.J. (Eds.), Forensic Geoscience, Principles, Techniques and Applications, **232**, Geological Society Special Publication, London, 23–136.

POUCHOU, J.L. and PICHOIR, F. (1991) Quantitative analysis of homogeneous or stratified microvolumes applied to the model "PAP". In: HEINRICJH, K.F.J., NEWBURY, D.E. (eds). *Electron Probe Quantification.* Plenum, New York, London pp. 31-35.

RANTA, E., STOCKMANN, G., WAGNER, T., FUSSWINKEL, T, STURKELL, E., TOLLEFSEN, E. and SKELTON, A. (2018) Fluid-rock reactions in the 1.3 Ga siderite carbonatite of the Grønnedal-Ika alkaline complex, Southwest Greenland. *Contributions to Mineralogy and Petrology,* **173**,78, 1-26.

REYES, A.G. (2000) Petrology and mineral alteration in hydrothermal systems: from diagenesis to volcanic catastrophes. *United Nations University Geothermal Training Programme* 1998 – Report Number 18.

REYNOLDS, R. C. (1963) Matrix corrections in trace element analysis by Compton scattering. *American Mineralogist*, **48**, 1133-1143.

RIETVELD, H. (1969) A profile refinement method for nuclear and genetic structures. *Journal of Applied Crystallography.*, **2**, 65-71, doi:10.1107/S0021889869006558.

RITCHIE, J.D., JOHNSON, H., BROWNE, M.A.E. and MONAGHAN, A.A., (2003) Late Devonian-Carboniferous tectonic evolution within the Firth of Forth, Midland Valley, as revealed from 2D seismic reflection data. *Scottish Journal of Geology* **39**, 121–134.

TULLOCH, W. and WALTON, H.S. (1958) The Geology of the Midlothian Coalfield. *British Geological Survey*, 157 pp.

UNDERHILL, J.R., MONAGHAN, A.A. and BROWNE, M.A.E. (2008) Controls on structural styles, basin development and petroleum prospectivity in the Midland Valley of Scotland. *Marine and Petroleum Geology*, **25**, 100 -102.

UPTON, B. G. J., ASPEN, P. and CHAPMAN, N. (1983) The upper mantle and deep crust beneath the British Isles; evidence from inclusions in volcanic rocks. *Journal of the Geological Society, London.* **140**, 105-121.

UPTON, B.G.J., ASPEN, P., GRAHAM A. and CHAPMAN, N.A. (1976) Pre-Palaeozoic basement of the Scottish Midland Valley. Nature, 260, 517-518.

UPTON, B.G.J., ASPEN, P. and HUNTER, R.H. (1984) Xenoliths and their implications for the deep geology of the Midland Valley of Scotland and adjacent regions. *Transactions of the Royal Society of Edinburgh, Earth Sciences*, **75**, 71-74.

UPTON, B.G.J., ASPEN, P., GRAHAM, A. and CHAPMAN, N. (1976) Pre-Palaeozoic basement of the Scottish Midland Valley. *Nature*, **260** No.5551, 517-518.

UPTON, B.G.J., DOWNES, H., KIRSTEIN, L.A., BONADIMAN, C., HILL, P.G. and NTAFLOS, T. (2011) The lithospheric mantle and lower crust/mantle relationships under Scotland; a xenolithic perspective. *Journal of the Geological Society, London **168**, 873-885.*

UPTON, B.G.J., FINCH, A.A. and SLABY, E. (2009) Megacrysts and salic xenoliths in Scottish alkaline basalts: derivatives of deep crustal intrusions and small-melt fractions from the upper mantle. *Mineralogical Magazine,* **73**, 943-956.

WILLIAMSON, I.T. (2003) Garleton Hills, East Lothian (NT449 764 – NT520 763). In: Carboniferous and Permian igneous rocks of Great Britain north of the Variscan Front. D. Palmer (ed.) *Joint Nature Conservation Committee and the British Geological Survey*. Geological Conservation Review Series, 55-66, Edinburgh and Nottingham.

Text Figures:

Fig.1. General map showing major faults in SE Scotland. The horizontal dash ornamentation marks the aeromagnetic lineament that may coincide with a seaward extension of the Southern Upland Fault (After Max 1976). WF - Weaklaw Fault.

Fig.2. A sketch map of Weaklaw. Ornament on Weaklaw diagrammatically indicates concentration of cored bombs and their decrease eastwards towards their unconformable contact with the Garleton Hills Volcanic Formation.

Fig.3. View of one of the Hanging Rocks, a rocky prominence standing out from the vegetated sea-cliffs. The Hanging Rocks are composed of agglutinated lava spatter and composite bombs also exposed on the fore-shore. The country rocks are Visean Garleton Hills Volcanic Formation.

Fig.4a. 'White trap' agglutinate, inferred to be former basaltic spatter, metasomatized to a carbonate-/ clay-rich assemblage.

Fig.4b A volcanic bomb of metasomatised basanite containing high concentration of near-spherical dolomite-filled amygdales. Coin: 15 mm diameter.

Fig.4c. An angular metasomatised peridotite xenolith surrounded by altered lava.

Fig.4d. A metasomatized peridotite xenolith, surrounded by altered basaltic 'white trap, contains dark green schlieren interpreted as mineralised shear zones containing chrome-rich

clays. Several smaller peridotitic fragments, generally enclosed by 'white trap' (i.e. 'cored bombs') can be discerned.

Fig.5. A cut slice of metasomatised peridotite xenolith from Weaklaw showing a greenish foliation. Alongside, for comparison, is a slice of a fresh spinel lherzolite xenolith from Argentina reflecting the presumed appearance that the Weaklaw xenolith would have had pre-metasomatism.

Fig.6a. BSE (back-scattered electron) image of a homogenous spinel grain showing smoothly embayed margins. The less reflective material is ankeritic carbonate and the least reflective component is clay. The clay and carbonate (pseudomorphing olivines) show a crudely concentric zonation.

Fig. 6b. BSE image of a spinel grain showing the spongy nature of the margins. Spinel is light-grey, darker grey filling of fissures and pores is probably a hydrous Al-Si clay mineral.

Fig.7. A high-magnification image of contrasted clays in the green schlieren from a re-crystallised lherzolite xenolith. The more rectilinear crystals to the left, mainly composed of SiO_2, Al_2O_3 and c. 10 wt% Cr_2O_3, are identified as kaolinite whereas those with more crinkly forms to the right are smectites with higher contents of MgO and approximately 30 wt% Cr_2O_3.

Fig.8. Multi-element data for a) the metasomatised peridotite and b) metasomatized basalt, normalised against corresponding values for unaltered peridotite and basanite samples taken *c*. 1 km to the east. The diagrams illustrate the elemental gains and losses incurred by the metasomatism. Note the overall enrichment in all the selected trace elements (except Ni) in the 'peridotite' and the general depletion of Ba and Sr in the ' basanite', relative to the other trace elements.

Fig.9a. Tuffisite cutting Weaklaw ejecta.

Fig.9b. A polished surface of a sample from the tuffisite dyke. The angular white clasts, composed mainly of kaolinite, are considered to represent altered alkali feldspar.

Tables

Table 1. Electron micro-probe analyses of spinel in xenolith WV 21 with analyses of spinel from the (fresh) spinel lherzolites at Brigs of Fidra (Downes *et al*., 2001) and Ruddon's Point, Fife (Upton *et al*., 2011) for comparison.

Table 2. XRF analyses of the chrome-rich clay concentrates from schlieren in a metasomatised peridotite xenolith.

Table 3. XRF whole-rock analyses of metasomatised-basanite host and metasomatised-peridotite xenoliths with analyses of unaltered basanite and peridotite (analogues from Brigs of Fidra east of the Weaklaw occurrences). Also analyses of the axial (columns 7 & 8) and marginal facies (column 9) of the younger tuffisite dyke.

TABLE 1. Spinel compositions in Weaklaw metasomatised peridotite compared to spinel compositions from Fidra and Ruddon's Point (Upton et al., 2011).

	Weaklaw			Fidra		Ruddon's Point	
Sample	WV21	10/1	1/1	Fd 1	Fd 2	14-9/1	86.1
SiO_2	0.05	0.04	0.07	0.04	0.07	0.03	0.06
TiO_2	0.15	0.13	0.13	0.20	0.66	0.01	0.08
Al_2O_3	59.74	59.17	60.06	54.93	55.82	56.52	57.91
Cr_2O_3	8.64	8.71	8.55	9.27	9.91	9.83	9.44
FeO^T	10.07	10.18	10.09	17.32	11.60	10.57	10.97
MnO	0.07	0.07	0.12	0.24	0.08	0.07	0.07
NiO	0.43	0.35	0.38	0.29	0.36	0.36	0.41
MgO	21.15	21.57	20.84	17.51	19.90	21.03	21.19
Total	100.30	100.22	100.24	99.80	98.56	98.42	100.13

TABLE 2. XRF analyses of chromian-smectite concentrations.

	Evaporite	Pressed powder pellet	Clay fraction < 2 µm)
SiO_2	25.78	29.55	46.23
TiO_2	0.18	0.42	0.16
Al_2O_3	3.91	10.55	18.93
Fe_2O_3	10.34	8.53	4.44
MnO	0.50	0.33	nd
MgO	9.56	6.54	2.75
CaO	21.24	11.16	1.43
Na_2O	nd	nd	nd
K_2O	0.19	0.69	0.79
Cr_2O_3	0.01	1.08	3.10
LOI	26.72	31.15	22.17
P	nd	<45	1082
Ni	614	477	2432
Cr	11360	7385	21235
V	263	175	348
Sc	22	33	36
Co	nd	59	158
Cu	24	25	38
Zn	68	67	58
Ga	nd	26	81
Rb	44	80	53
Sr	104	129	28
Zr	23	27	54
Nb	1.9	<1	<1
Y	4	<0.5	<0.5
Mo	nd	<1.5	12
Cs	nd	7	7
Ba	1105	1488	129
Hf	nd	<0.4	3
Hg	nd	<30	<30
La	4	8	<0.5
Ce	nd	<1	<1
Nd	nd	<0.5	<0.5
Pb	0.9	<0.5	633
U	nd	<0.3	<0.3
Th	4.3	<0.2	<0.2

TABLE 3. Whole-rock analyses of metasomatised peridotite and basalts from Weaklaw vent compared to those of unaltered equivalents from Brigs of Fidra.

	Peridotitic			*Basaltic*			*Tuffisite*		
	1	2	3	4	5	6	7	8	9
wt.%									
SiO_2	8.14	13.33	43.97	14.99	10.19	44.37	57.63	48.32	10.67
TiO_2	0.19	0.37	1.13	1.70	1.51	2.94	0.27	0.18	0.07
Al_2O_3	4.11	6.11	3.94	8.55	6.91	14.12	23.99	19.79	4.34
Fe_2O_3	11.38	13.23	9.01	7.48	8.20	12.80	3.25	5.19	11.11
MnO	0.52	0.57	0.13	0.44	0.94	0.18	0.07	0.12	0.78
MgO	11.80	14.04	38.87	10.23	10.85	9.58	0.03	2.88	4.49
CaO	25.32	28.94	3.35	21.97	24.42	9.83	3.04	6.40	33.76
Na_2O	0.06		0.56	0.01	0.09	3.03		0.08	0.09
K_2O	0.08	0.16	0.15	0.67	0.35	0.81	0.25	0.15	0.09
P_2O_5	0.14	0.06	0.02	0.77	1.00	0.63	0.12	0.07	0.04
LOI	38.20	23.01		32.55	35.55	1.49	11.28	16.31	34.18
Total	99.82	99.73	100.03	99.36	99.82	99.78	99.59	99.49	99.62
Ni	800.0	887.2	2018.0	309.0	219.0	188.1	51.6	83.0	348.0
Cr	3425.0	4079.4	2774.0	256.0	229.0	261.9	4.1	2.7	3.9
V	117.0	187.2	78.0	162.0	169.9	226.3	39.9	44.0	73.0
Sc	19.0	25.0	14.0	17.0	19.9	23.7	nd	1.5	7.0
Cu	24.0	74.5	46.0	83.0	163.6	60.1	123.9	13.7	17.2
Zn	40.0	201.5	59.0	79.0	105.2	105.5	27.8	56.8	292.0
Rb	8.0	8.4	3.9	13.0	6.9	10.9	10.1	7.6	6.6
Ba	33.0	49.0	10.0	82.0	95.7	780.0	283.3	55.2	3.2
Sr	100.0	94.6	16.9	171.0	163.4	1034.5	65.0	65.4	179.0
Zr	34.0	47.3	6.0	143.0	125.1	266.6	2558.8	2020.0	478.0
Nb	3.0	4.4	0.5	32.0	29.0	61.6	304.7	213.0	55.8
Y	10.0	8.0	3.7	23.0	26.5	29.1	177.8	138.0	31.5
La	10.0	10.4	0.7	41.0	50.0	47.9	212.9	158.0	80.4
Ce	24.0	29.8	1.2	79.0	93.8	87.3	434.1	340.0	137.0
Nd	14.0	14.7	0.8	37.0	43.3	41.7	169.6	132.0	50.8
Pb	698	465.6	0.5	49.0	6.7	nd	6.2	7.1	7.6
U	nd	0.3	nd	37.0	10.4	nd	4.6	2.9	0.4
Th	nd	nd	nd	2.8	2.3	nd	56.3	46.3	9.9

1) WL21 Meta-somatised peridotite; 2) WL31 Meta-somatised peridotite; 3) Peridotite; Brigs of Fidra (data from Downes *et al.*, 2011) ; 4) WL32 Meta-somatised basalt ('white trap'); 5) WL33 Meta-somatised basalt ('white trap'); 6) BOF 10 Basanite, Brigs of Fidra; 7) WL28 Speckled tuffisite; 8) WL29 Speckled tuffisite; 9) WL30 Brown tuffisite.

Figure 1

Click here to access/download;Figure;Fig. 1 Weaklaw Map.png

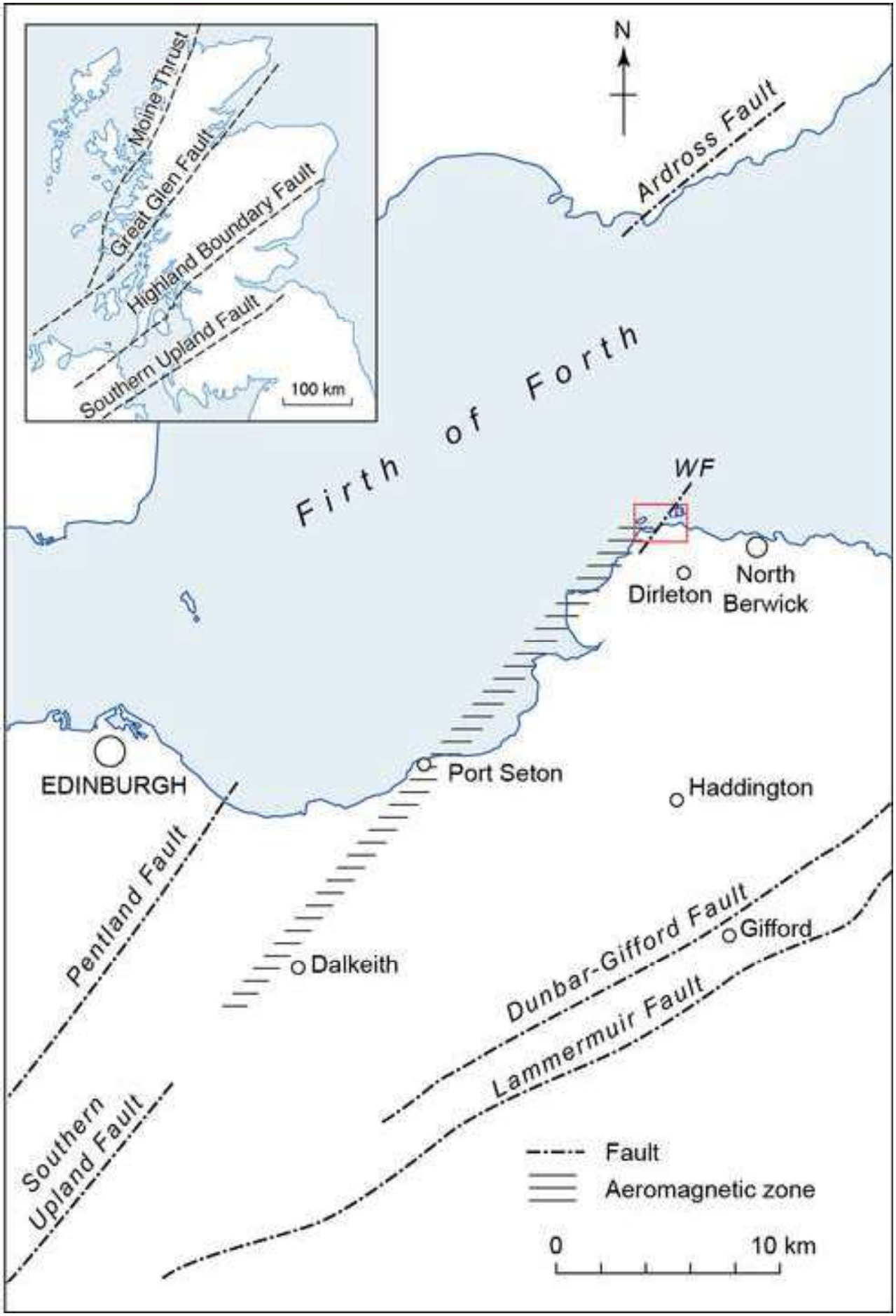

Figure 2

Click here to access/download;Figure;Fig 2. Weaklaw_New.png

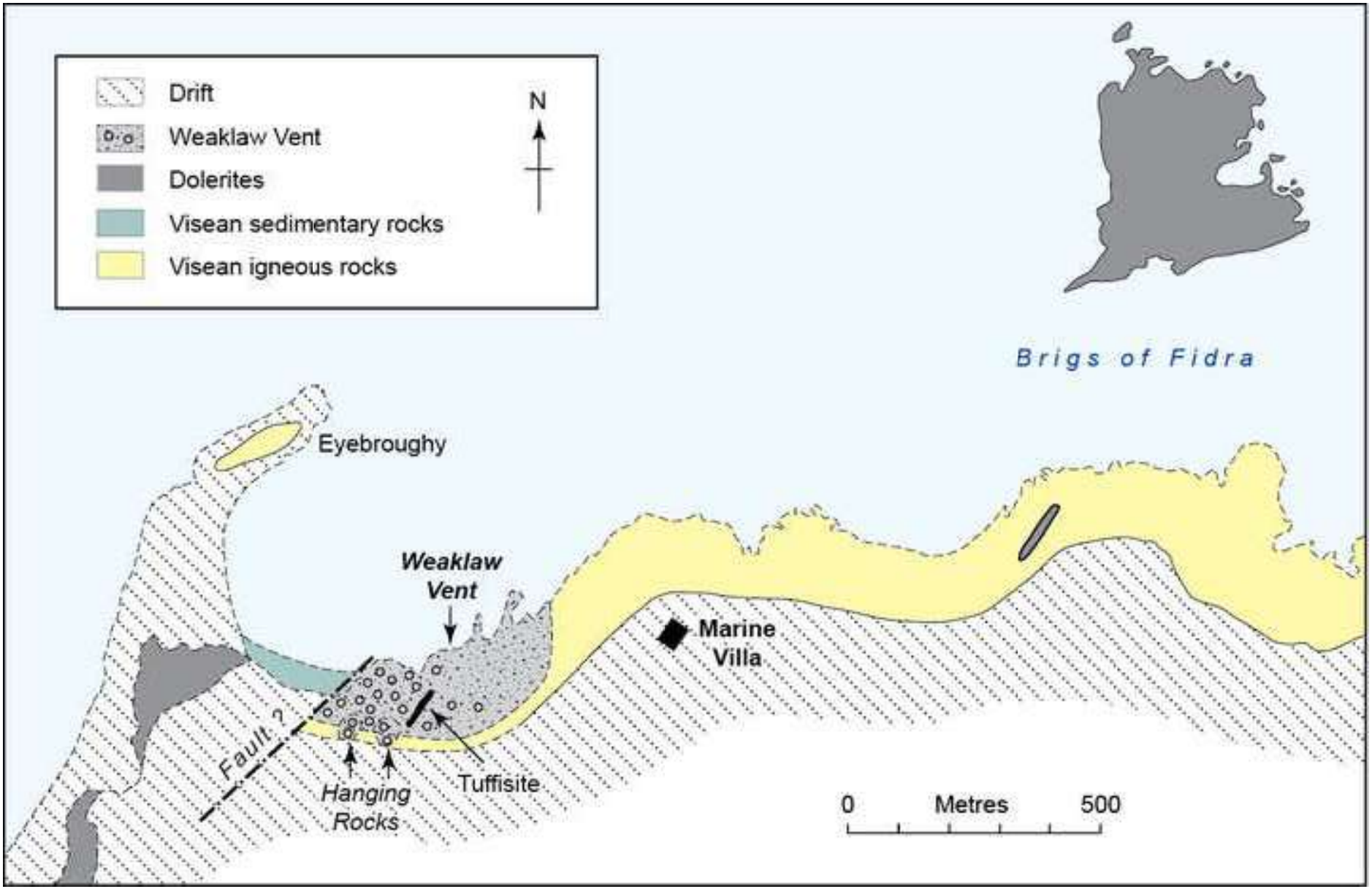

Figure 3

Click here to access/download;Figure;Fig. 3 Hanging rocks new.JPG

Figure 4a

Click here to access/download;Figure;Fig. 4a Weaklaw agglutinate with peridotites.JPG

Figure 4b

Click here to access/download;Figure;Fig. 4b vesiculated meta-basalt.JPG

Figure 4c

Click here to access/download;Figure;Fig. 4c Mantle xeno with basaltic frame (004).jpg

Figure 4d

Click here to access/download;Figure;Fig. 4d Foliated peridotite in cored bomb.jpg

Figure 5

Click here to access/download;Figure;Fig. 5 Weaklaw metaperid & fresh sp lherzolite 1.JPG

Figure 6a

Click here to access/download;Figure;Fig. 6a Spinel BSE.tif

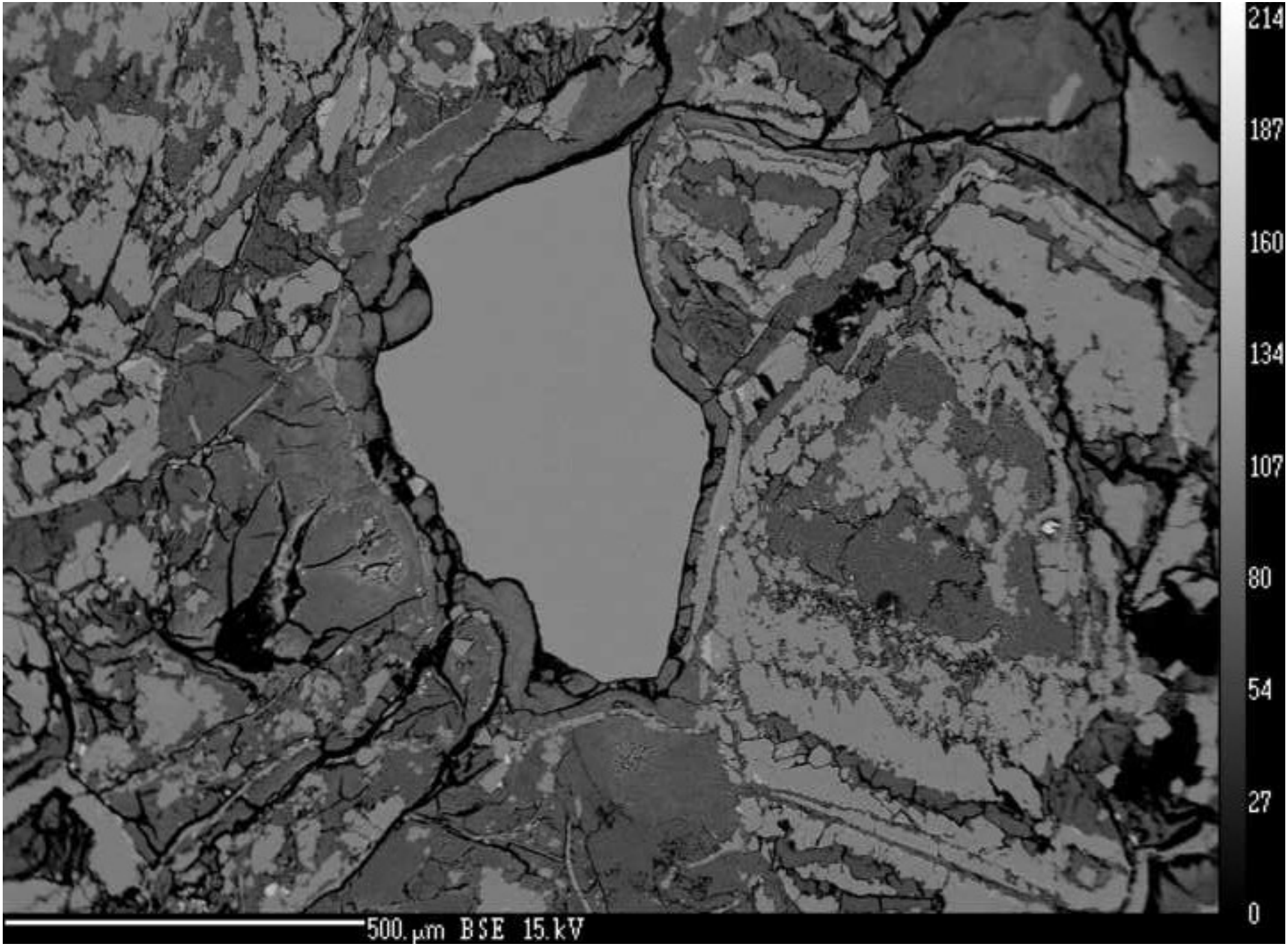

Figure 6b

Click here to access/download;Figure;Fig. 6b BSE of spinel Weaklaw.tif

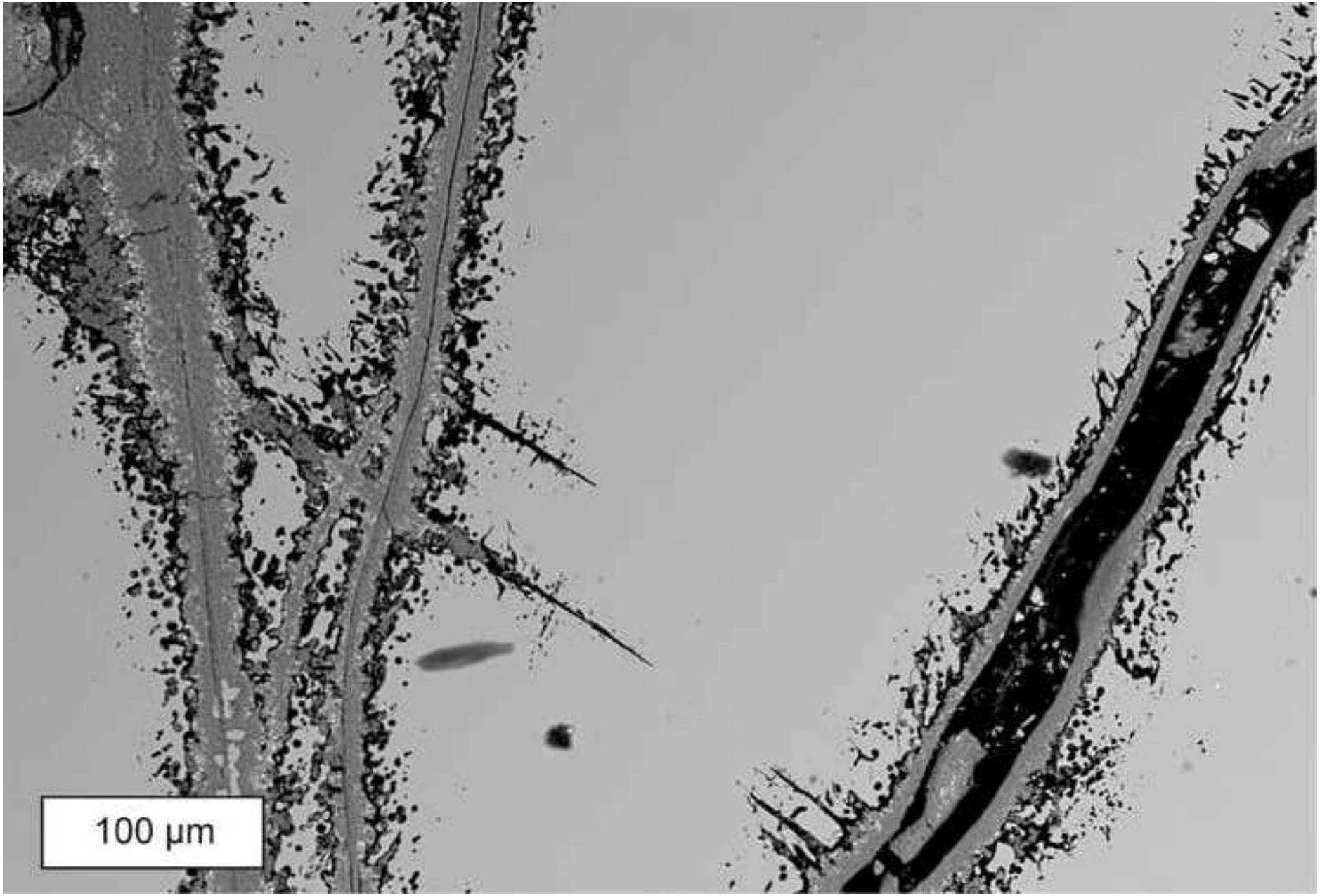

Figure 7

Click here to access/download;Figure;Fig. 7 Clays.tif

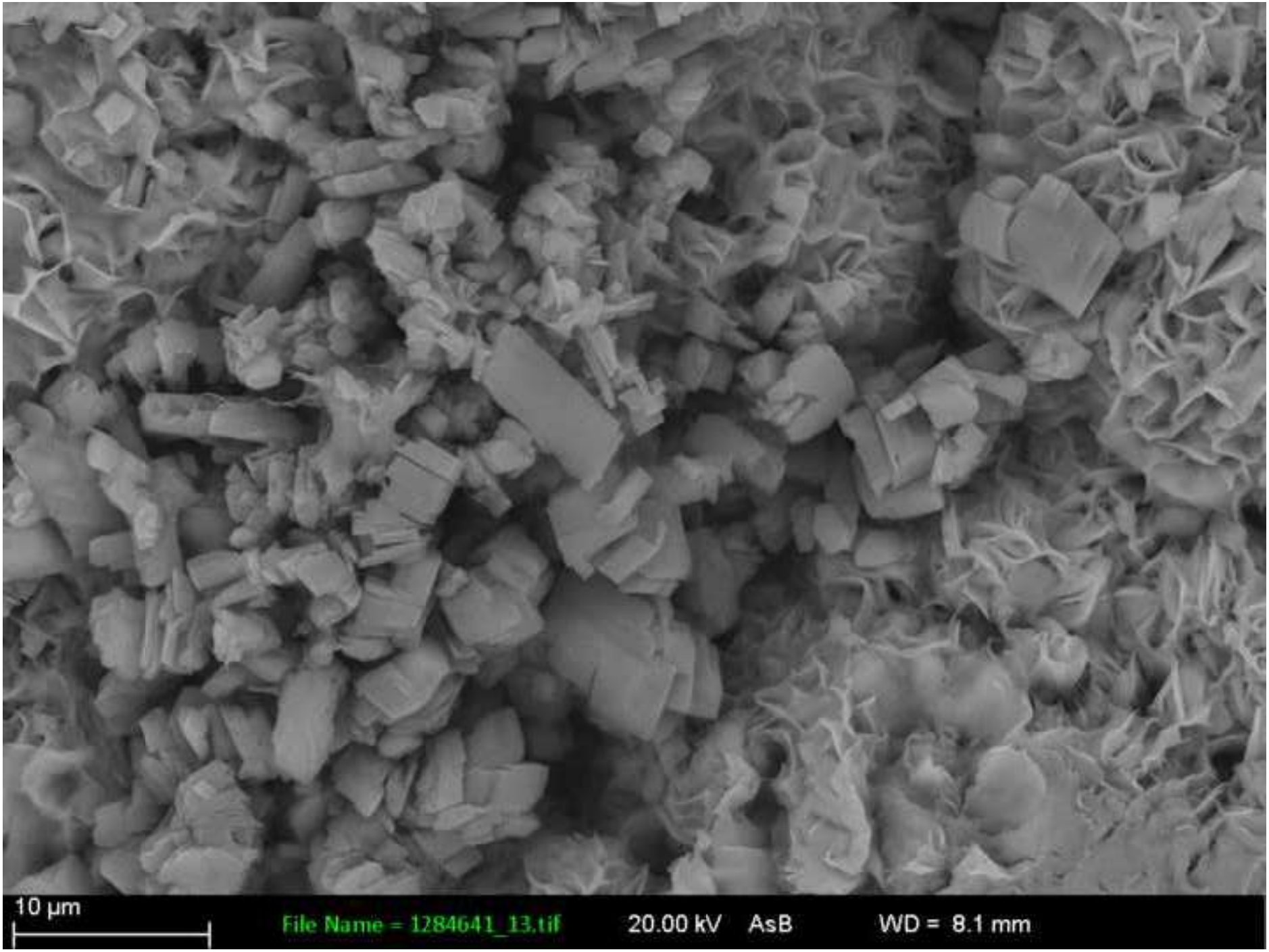

Figure 8

Click here to access/download;Figure;Fig. 8 Weaklaw data norm.jpg

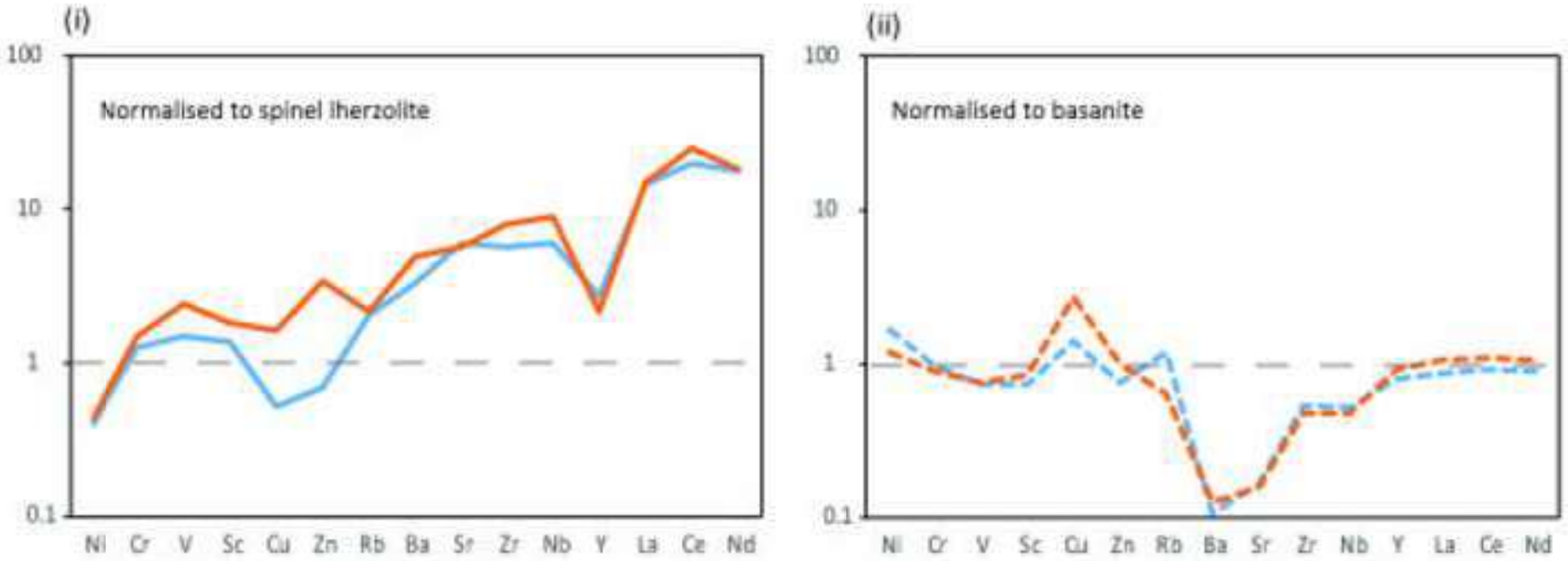

Figure 9a

Click here to access/download;Figure;Fig. 9a Tuffisite_field.jpg

Figure 9b

Click here to access/download;Figure;Fig. 9b Speckled dyke.jpg